(Received 25 April 2024, Accepted 14 June 2024, Scheduled 19 July 2024)

Reconfigurable Compact Wide-Band Quad-Port Antennas Based on a Varactor Diode for Sub-6 GHz 5G Communications

Qasim Hadi Kareem Al-Gertany*

Electrical Engineering Department, Al-Iraqia University, Baghdad, Iraq

ABSTRACT: The rapid expansion of wireless communication systems has spurred a growing demand for adaptable multiple-input multiple-output (MIMO) antennas capable of accommodating diverse frequency bands and operational environments. This paper presents a compact quad-port wide-band tuning-reconfigurable MIMO antenna tailored specifically for 5G applications operating within the sub-6 GHz spectrum. The proposed design enhances isolation levels (> 18 dB) and augments pattern diversity by utilizing four orthogonal radiating elements. Integrating a C-shaped monopole element with a matching stub facilitates frequency tuning via a varactor diode, ensuring a consistent radiation pattern. The lower and upper resonant bands could be fine-tuned by adjusting the varactor diode's reverse-biased voltage within the allowed range of 0.5 to 10 V. These bands are 4 to 5.18 GHz and 5.45 to 6.65 GHz, respectively. The proposed antenna system's four C-shaped elements are placed on a $40 \times 40\,\text{mm}^2$ ground plane and mounted on a Rogers RT5880 substrate that is 0.8 mm thick with a relative permittivity of 2.2. This design is well suited for various wireless applications and cognitive radio networks due to its compatibility with sub-6 GHz frequency bands and wide-band tuning capabilities.

1. INTRODUCTION

The primary objective of modern communication equipment is to accommodate a diverse range of wireless standards, ensuring rapid data transmission. Among the several technologies available, the MIMO system emerges as a notable solution for improving coverage and data throughput due to its inherent frequency variety. Recent research has investigated many methods for reducing the size of antennas, operating in multiple frequency bands, and achieving a wide range of frequencies [1, 2]. Nevertheless, the interconnection between resonating parts is a significant obstacle in MIMO antenna designs, especially densely arranged. Various strategies are employed to address this coupling issue. These strategies include defective ground structures (DGSs), parasitic reflectors, decoupling devices like split-ring resonators (SRRs), and neutralization lines [1–3].

The rapid development of various services has caused congestion inside the frequency band, leading to elevated spectrum licensing expenses and increasing customer per-bit rates. To solve these problems, frequency reconfigurable MIMO antenna systems are a good idea. They make it possible to send large amounts of data quickly while making good use of spectrum resources for many different wireless protocols [4]. These antennas at the front ends of cognitive systems enable smooth and interference-free radiation by allowing seamless transitions across different bands.

This work primarily aims to design and fabricate antennas that can manipulate both frequency and radiation pattern, with a particular focus on investigating the incorporation of a varactor diode as the tuning element. Existing literature has documented several frequency-reconfigurable antennas functioning within the range of 1.8–4.5 GHz [5–15]. A significant proportion of published research on reconfigurable antennas focuses on single-patch element configurations, which frequently encounter bandwidth and dimension limitations. On the contrary, wireless technologies that depend on broad bandwidths to transmit data efficiently can benefit substantially from implementing frequency-reconfigurable MIMO antenna systems. These systems can modify their operational frequencies in response to changing circumstances, improving flexibility in various communication scenarios. The existing literature has documented various designs for frequency-reconfigurable MIMO antennas [16–20].

The literature has extensively studied two-element reconfigurable MIMO systems due to their ability to improve data rates and channel capacity. Incorporating antenna elements enhances system performance, resulting in enhanced overall efficiency. Prior research has presented MIMO antennas with four radiators, demonstrating the continuous investigation in this field [21–29]. [21] presents a 4-element dual-mode meandered F-shape reconfigurable MIMO antenna for cognitive radio applications. The antenna combines PIN and varactor diodes to cover the frequency bands 743–1240 and 2400 MHz. Isolation equals 12 dB across operation bands with a $65 \times 120\,\text{mm}^2$ surface area. [22] presents a 4-element MIMO antenna system with tuning capability for WiMAX and cognitive radio applications. Varactor diodes are used to electronically achieve reconfigurability by changing the pentagonal slot antenna's capacitance. The antenna is tuned to cover the frequency band from 3.2 GHz to 3.8 GHz with $60 \times 120\,\text{mm}^2$ board dimensions. [23] proposes a four-port hexagonal antenna with a

* Corresponding author: Qasim Hadi Kareem (qasim.hadi2017@gmail.com).

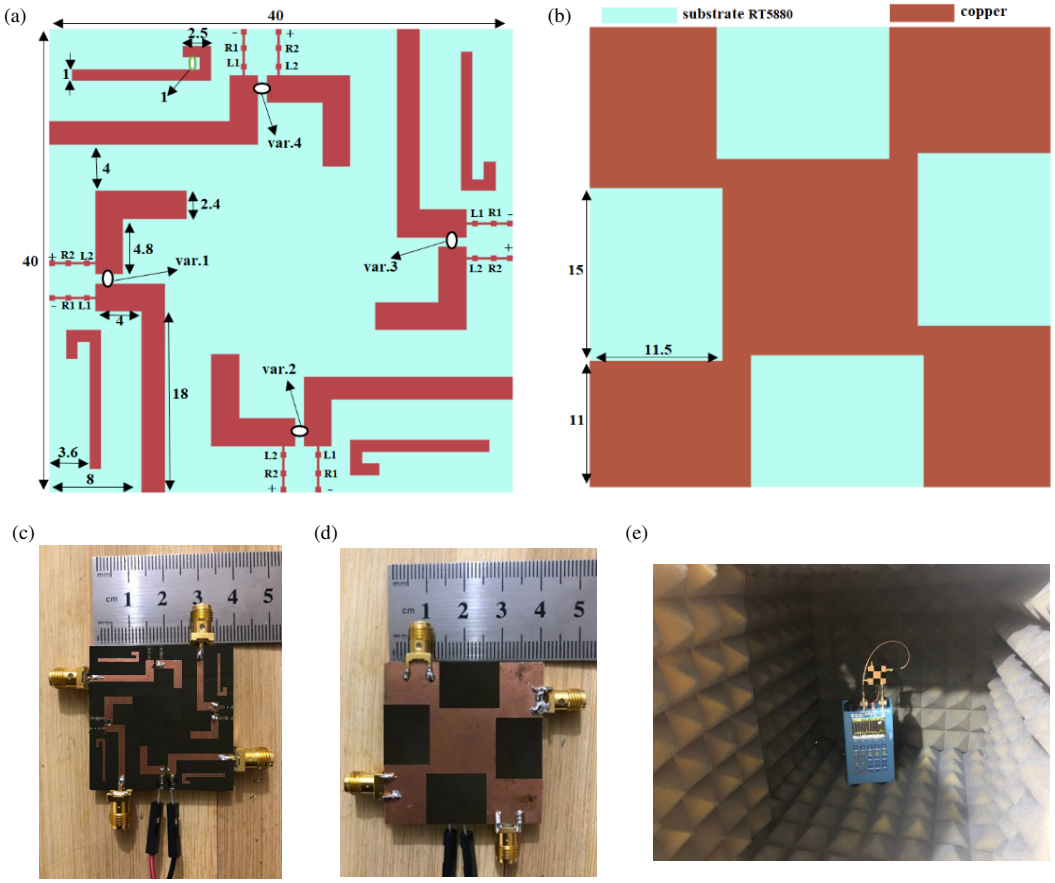

FIGURE 1. Geometry of wide-band MIMO antennas: (a) Four-elements front view and (b) back view, (c)–(e) fabricated prototype (top, bottom, and anechoic chamber view).

$120 \times 60\,\text{mm}^2$ substrate area. The feedline integrates a varactor diode to achieve reconfigurable characteristics from 1.3 to 2.6 GHz while maintaining an isolation of 12 dB for the operating band.

Ref. [24] proposes a quad-port MIMO antenna with a $50 \times 50\,\text{mm}^2$ surface area based on an octagonal ring shape and a tunable frequency. Each element employs a varactor diode in its center to enable frequency reconfigurability. Rectangular DGS gaps are used for isolation enhancement over the operating band (4.55 to 5.56 GHz). With a printed circuit board (PCB) board size of $90 \times 90\,\text{mm}^2$, [25] presents four ultra-wideband (UWB) monopole elements in the shape of an annular ring, arranged orthogonally. With the feed line and stepped impedance resonating stub (SIRS) connected, PIN diodes convert the wideband to narrowband signal for every monopole element. The reconfigurable frequency states are UWB, mid-band (5G), and WLAN. Ref. [26] illustrates four rectangular monopoles with an overall size of $70 \times 70\,\text{mm}^2$, which are orthogonally placed, split into two patches, and connected by a DGS. By placing an RF PIN-diode between the upper and lower patches, it is possible to enable the frequency diversity function, and the upper patch uses a split-ring resonator to cover a variety of sub-6 GHz application bands. For cognitive radio underlay and interweave applications, [27] introduces a four-element frequency reconfigurable antenna with a $50 \times 38\,\text{mm}^2$ PCB area. When the five PIN diodes in the sensing antenna and four PIN diodes in the communication antenna are in the correct states, eighteen MIMO modes are available. However, supplementary components in the biasing circuit added complexity to the production process.

Ref. [28] presents a quad-port, multi-polarized switchable antenna for sub-6 GHz applications. This antenna, incorporating four PIN diodes, operates within the 3–5 GHz range and occupies an area of $65 \times 65\,\text{mm}^2$, providing only circular polarization (both LHCP and RHCP). Similarly, [29] describes quad-port antennas designed for indoor wireless communications, utilizing a substrate size of $68 \times 68\,\text{mm}^2$ and eight PIN diodes to function within 2–6 GHz; however, the increased number of diodes and high-profile system complexity presents design challenges.

Previous works focused on narrow bandwidth, non-continuous tuning in frequency, a lack of reconfigurable compact planes, high-profile designs, and poor isolation for radiating elements. To overcome these limitations, this paper proposes a wide-band, continuously tunable, highly isolated frequency-tunable MIMO antenna with a C-shaped monopole design based on a connected ground structure. Each element has a varactor diode for reactive loading, which allows bias voltage to change from 4 to 6.65 GHz. The four antennas, supported by strip lines and a C-shaped element

with associated ground structure, are the smallest and most isolated frequency-tunable multiple antenna arrangements. The lower resonant band of the antenna can be adjusted within the frequency range of 4 to 5.18 GHz, resulting in an isolation of approximately 20 dB. Similarly, the upper band of the antenna can be fine-tuned from 5.45 to 6.65 GHz, yielding an isolation of 18 dB. The antenna's planar construction, compact dimensions, and wide tuning make it well suited for front-end solutions in wireless communications.

2. ANTENNA DESIGN

Figure 1 illustrates the antenna design, including the feeding network for the varactor diode and the fabricated prototype. It presents both the front and back views of the design. The system consists of four C-shaped monopole antennas on a $40 \times 40\,\text{mm}^2$ ground plane. The ground plane is implemented on a Rogers RT5880 substrate with a thickness of 0.8 mm. The substrate has a relative permittivity 2.2 and a tangent loss 0.0009. Four radiating elements in the shape of a C make up the configuration, positioned orthogonally to achieve sufficient isolation and share a common ground.

The design includes a main radiator for lower frequencies and a parasitic L-shaped radiator for higher frequencies. The interconnection between these radiators is substantial, posing difficulties in autonomously regulating each frequency range. Equations (1) and (2) compute the size of the usual 50-ohm microstrip transmission line, which drives each monopole antenna. Figure 1(a) shows that we maintain a gap of 0.8 mm to place a varactor diode between the central radiator and the L-shaped parasitic radiator. Furthermore, Figure 1(b) demonstrates that a partial ground plane on the opposite side of the substrate supports each radiator in the MIMO system. The interconnection of the ground plane of each monopole antenna enables the construction of a shared ground plane, hence offering advantages for MIMO antennas.

The proposed MIMO antenna design employs a varactor diode (SMV 2019) for tuning. Each varactor diode is placed within the space that divides the L-shaped radiator from the rectangular patch radiator to maximize efficiency. For the varactor diode configuration (var.1–var.4 in Figure 1(a)), the anode is connected to an L-shaped parasitic radiator and the cathode to the central radiator.

A feeding network in Figure 2 is established to supply the varactor diodes with a reverse-biased voltage. This network

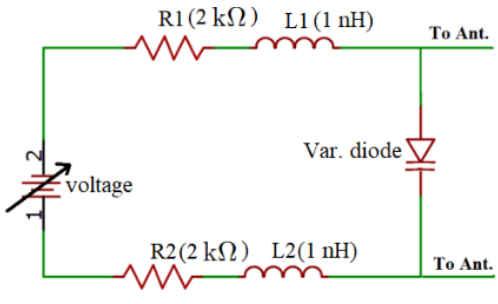

FIGURE 2. Feeding network for varactor diode.

comprises an inductor ($L_{1,2}$) and a resistor ($R_{1,2}$). A variable DC power source is linked to the cathode of every varactor diode through the feeding network. Every feeding network contains a resistor ($R_{1,2}$) to control the input current of the varactor diode. We use a very tolerant high-Q inductor ($L_{1,2}$) for the RF choke.

Standard equations are used to determine the initial dimensions of the effective length of the monopole antenna. Then, the antenna's performance is refined by obtaining optimal values through parametric analysis, which is helped by a full-wave electromagnetic simulator [30].

$$\varepsilon_{eff} = \frac{\varepsilon_r + 1}{2} + \frac{\varepsilon_r - 1}{2}\left(1 + 12\,\frac{h}{W}\right)^{-0.5} \tag{1}$$

$$L_{f_r} = \frac{c}{4 f_r \sqrt{\varepsilon_{eff}}} \tag{2}$$

where ε_{eff} and ε_r are the effective and related permittivity of the material; c is the speed of light in a vacuum; h and w are the thickness and width of the substrate, respectively.

As illustrated in Figure 3, the methodology for designing antennas offers an in-depth description of the consecutive phases involved. In the first step, a 50-Ω strip line is utilized to supply power to the antenna. In step two, a stub is incorporated to achieve impedance matching. However, problems arise because the surface underneath the radiating patch antenna displays an inconsistent impedance, making it an inefficient radiator throughout the entire frequency range.

Further advancing the process, the third phase (step 3) is depicted in Figure 3(c). At this step, a stub links an L-shaped parasitic element to the main radiator, enabling its operation in a higher frequency range. The accompanying figure, Figure 4,

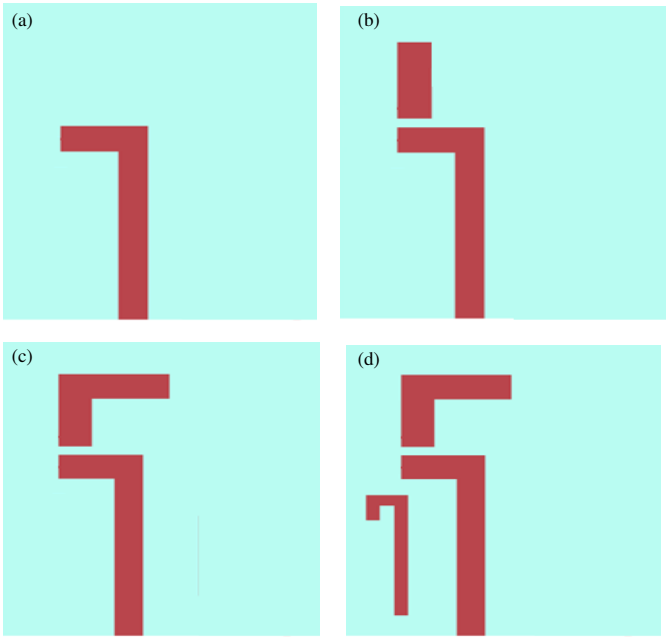

FIGURE 3. Methodology for proposed antennas. (a) Step 1; (b) Step 2; (c) Step 3; (d) Step 4.

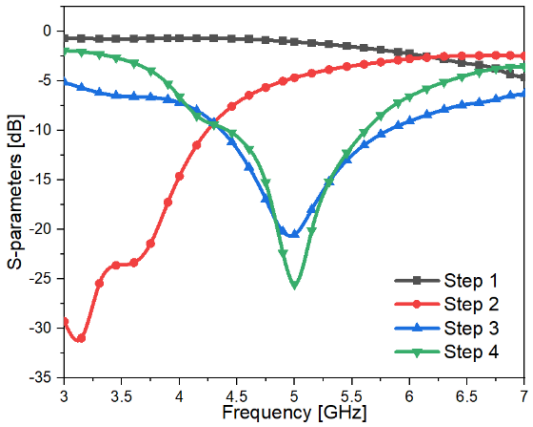

FIGURE 4. Design process for the reflection coefficient.

visually illustrates this configuration, offering distinct insight into this aspect.

In further progress, varactor diodes are accommodated in a precisely etched gap measuring 0.8 mm that separates the primary and parasitic L-shaped elements. The precise configuration, illustrated in Figure 3, in conjunction with a capacitance 1.5 pF enables the radiator to function without interruption at a resonance of 5 GHz. A curly patch is positioned adjacent to the radiator's edge to reduce return loss by matching the impedance of the patch and feed line. Figure 3(d), representing the fourth stage of the procedure, illustrates this improvement.

The crucial determinants of the varactor diode's placement are the intended operational frequency range, the physical design of the antenna, and the necessary impedance characteristics. By accurately locating the diodes along the radiating elements or feed structure, it becomes possible to fine-tune the impedance and resonance frequency of the antenna. As a result, this modification substantially impacts the bandwidth and effectiveness of the antenna.

According to the design objectives and requirements, the positioning of an independent varactor diode on an antenna is determined. Although it is feasible to adjust the location of the antenna, it is crucial to approach these modifications with a thorough comprehension of their effects on the overall performance.

An effective transfer of power from the transmission line to the antennas and synchronization of currents (electrical fields) are two radiating qualities that must be present for radiation to be efficient [24]. To do this, one must minimize the reactive components of impedance by utilizing an equivalent circuit. The corresponding circuit is depicted in Figure 5, which visually represents the LCR-sections for both the feed line and radiator element.

The circuit representing the printed monopole patch as a wide-band parallel LCR-circuit for its first resonant frequency is developed using fundamental transmission line theory [31]. The inductance L_2 and capacitance C_2 represent the printed monopole, while the inductance L_1 and capacitance C_1 represent the microstrip feed line. The radiation resistances of the element and the superstrate are denoted by the load resistances R_1 and R_2, respectively. The term "R_{in}" in the context of a

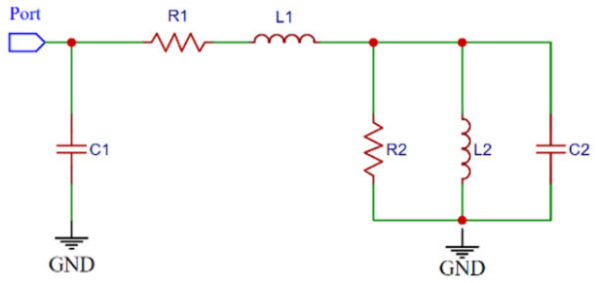

FIGURE 5. Equivalent circuit for feed-line and radiator.

port refers to the input impedance of the source, equal to 50 Ω. Equations (3) and (4) [32] establish the microstrip line's inductance and capacitance values.

$$L = \begin{cases} \frac{60l}{v_0} \ln\left[\frac{8h}{w} + \frac{w}{4h}\right] & \text{for } \frac{w}{h} \leq 1 \\ \frac{120\pi l}{v_0}\left[\frac{1}{\frac{w}{h}+1.393+0.667\ln\left(\frac{w}{h}+1.444\right)}\right] \end{cases} \tag{3}$$

$$C = \begin{cases} \frac{\epsilon_r l}{60 v_0 \ln\left[\frac{8h}{w}+\frac{w}{4h}\right]} & \text{for } \frac{w}{h} \leq 1 \\ \frac{\epsilon_r l\left[\frac{w}{h}+1.393+0.667\ln\left(\frac{w}{h}+1.444\right)\right]}{120\pi v_0} \end{cases} \tag{4}$$

In this context, variables l, w, ϵ_r, h, and v_0 represent the length, width, relative permittivity, height, and velocity of electromagnetic waves in free space, respectively. The equations provided yield the values of L_1, C_1, L_2, and C_2.

The frequency of the printed monopole antenna may be determined by considering the values of L_2 (0.67 nH) and C_2 (1.5 pF). This allows for the antenna's resonant frequency to be equal to the frequency of the LC-circuit, as described by Equation (5).

$$f_r = \frac{1}{2\pi\sqrt{L_2 C_2}} \tag{5}$$

Here, 5 GHz is the antenna's resonance frequency.

The comparison between the responses produced from circuit simulation and Computer Simulation Technology (CST) simulation is presented in Figure 6. The response of the equivalent circuit in advanced design system (ADS) exhibits a frequency shift towards the higher end and a wider bandwidth

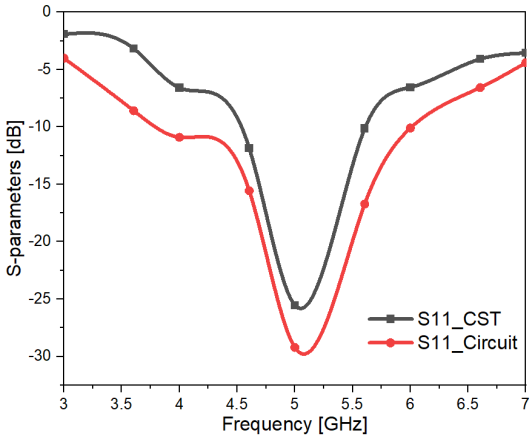

FIGURE 6. Response circuit using CST and ADS.

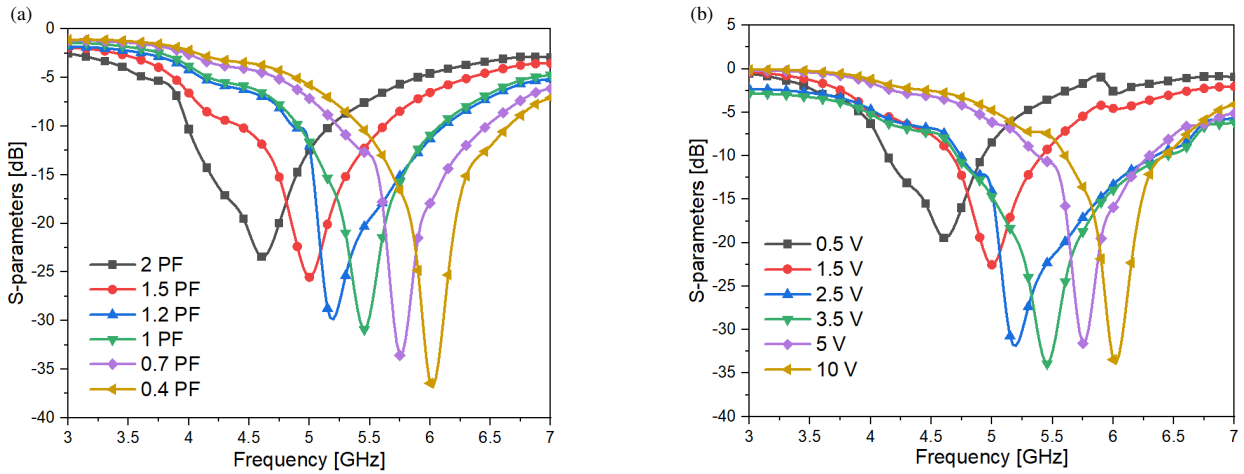

FIGURE 7. Reflection coefficient: (a) Simulated and (b) measured.

compared to the response using CST. Each terminal has an impedance of 50 ohms. It accurately estimates equivalent values from ADS.

The impedance matching and resonance frequency are immediately affected by variations in inductance, resulting in a consequential influence on its bandwidth with minimum modifications. In contrast, changes in capacitance significantly impact both the range of frequencies and bandwidth values. To attain the highest level of performance within the specified frequency range, it is imperative to maintain an appropriate balance between inductance and capacitance.

3. RESULTS AND DISCUSSIONS

3.1. S-Parameters

The simulation and optimization of a reconfigurable quad-port antenna design were carried out using a full-wave electromagnetic simulator, CST. The evaluation of the reflection coefficient conducted using the CST tool is depicted in Figure 7(a). As described in the datasheet, the frequency tuning experiment entailed modifying the varactor diode's capacitance values within the parameter range of 0.4 to 2 pF.

A system prototype was created to verify the simulation results received from CST. Figures 1(c)–(e) display this experimental model. A KC901V model vector network analyzer (VNA) was used to perform the measurements extending from 100 MHz to 7 GHz in frequency. Before measurement, the VNA experienced a quick open/short/load calibration operation. A more straightforward method for measuring the transmission and reflection coefficients has been developed: varying the reverse bias voltage applied to the diode from 0.5 to 10 V. According to the datasheet, the varactor diode SMV2019 has a minimum of 0 V bias voltage. The result is a 0.25 GHz drop in resonance frequency.

Figure 7 illustrates a comparison test of the reflection coefficient, comparing the simulated and measured values. Increasing the varactor diode's reverse biased voltage from 0.5 to 10 V changed the lower resonant band from 4 to 5.18 GHz and the higher band from 5.45 to 6.65 GHz.

This section focuses on three specific voltage scenarios, particularly 0.5 V, 2.5 V, and 10 V, to enhance clarity and facilitate comprehension. The simulated antenna exhibited a frequency range of 5.45 to 6.65 GHz, with a bandwidth (BW) of 1.2 GHz for the upper resonant band, resulting in a fractional BW of 20% at 0.4 pF. Likewise, when the capacitance value was set to 1 pF, the simulated antenna functioned within the 5 to 6 GHz frequency range. The center resonant band exhibited a 10-dB BW of 1 GHz, indicating a fractional BW of 18%. At 2 pF, the simulated antenna functioned within the 4 to 5.18 GHz frequency range, demonstrating a BW of 1.18 GHz for the lower resonant frequency and a fractional BW of 26.2%.

Additionally, Figure 8 presents the transmission coefficient (S_{12}) that was measured and simulated for identical three voltage occurrences. The observed transmission and reflection coefficients exhibited a remarkable degree of alignment with the anticipated values. Slight differences in resonance frequency and bandwidth can be caused by manufacturing flaws, parts that get clumped together in the biasing network, soldering errors in the diodes, and problems with the SMA or cable.

3.2. Evaluation of the Proposed Design's Diversity Performance

The evaluation of diversity performance in MIMO antennas can be achieved by utilizing the envelope correlation coefficient (ECC) and diversity gain (DG). Using the ECC computation enables the assessment of the spatial correlation or diversity extent between two identical antennas. Using the ECC computation, the spatial correlation or diversity extent between two identical elements can be assessed. When MIMO antennas have low efficiency, it is not possible to use S-parameters for ECC computation [33]. Therefore, in the case of these antennas, the estimation of ECC is obtained by analyzing the radiation patterns in the distant field. On the other hand, evaluating ECC for high-efficiency antennas entails analyzing the relationship between losses. This methodology is especially well suited for MIMO antennas with a radiation efficiency surpassing 50%. The equa-

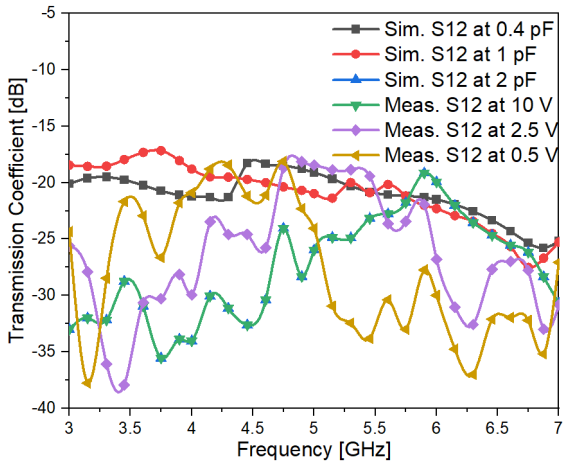

FIGURE 8. Simulated and measured transmission coefficient.

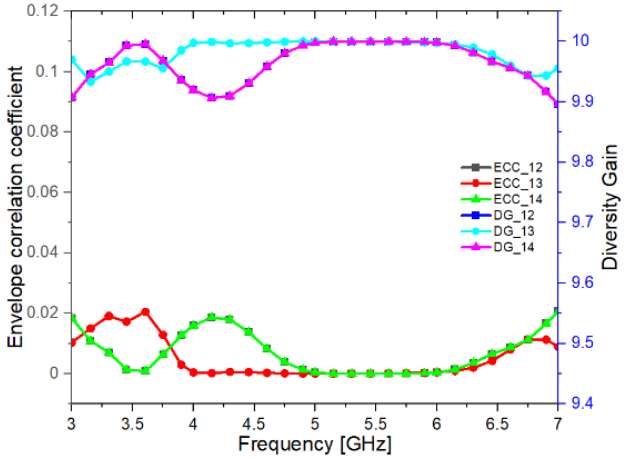

FIGURE 9. ECC and DG of quad-port antenna.

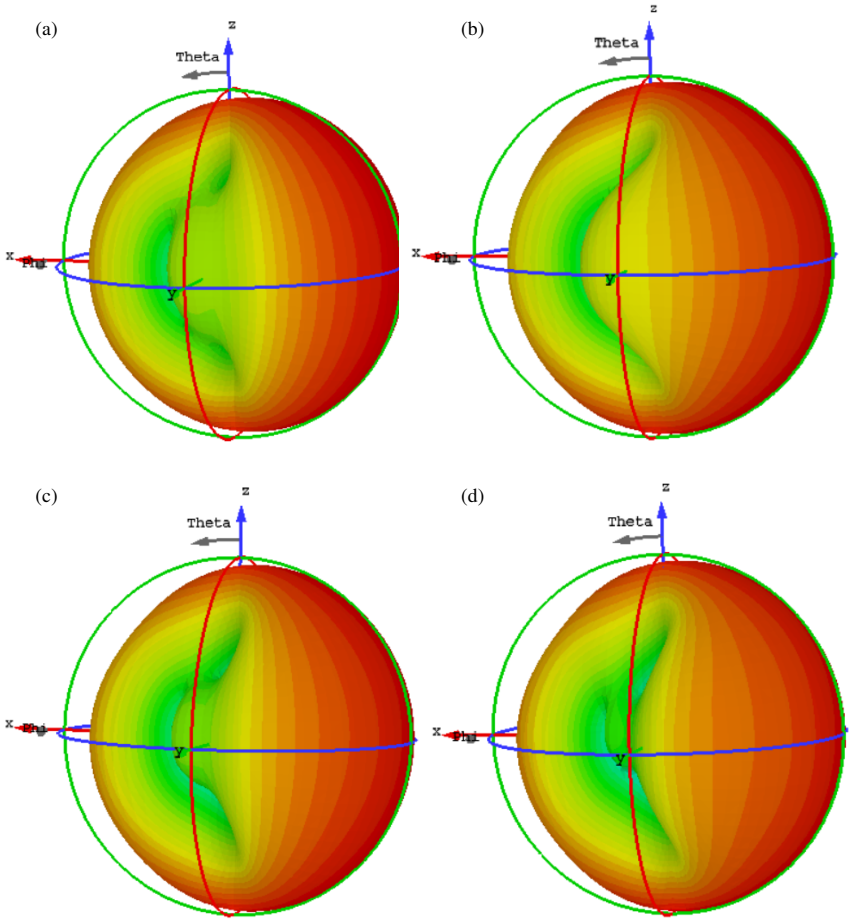

FIGURE 10. 3-D electric-field radiation patterns: (a) At 5 GHz; (b) At 5.25 GHz; (c) At 5.5 GHz; (d) At 6 GHz.

tion in [33] can be utilized to calculate the assured correlation coefficient.

$$|\rho_{ij}|_{\text{guaranteed}} = |\rho_{ij}| + \sqrt{\left(\frac{1}{\eta_i} - 1\right)\left(\frac{1}{\eta_j} - 1\right)} \quad (6)$$

where

$$\rho_{ij} = \frac{-s_{ii}s_{ij}^* - s_{ji}s_{jj}^*}{\sqrt{\left(1 - |s_{ii}|^2 - |s_{ji}|^2\right)\left(1 - |s_{jj}|^2 - |s_{ij}|^2\right)\eta_i\eta_j}} \quad (7)$$

The symbols η_i and η_j denote the first and second antennas. Once the correlation coefficient has been determined, the

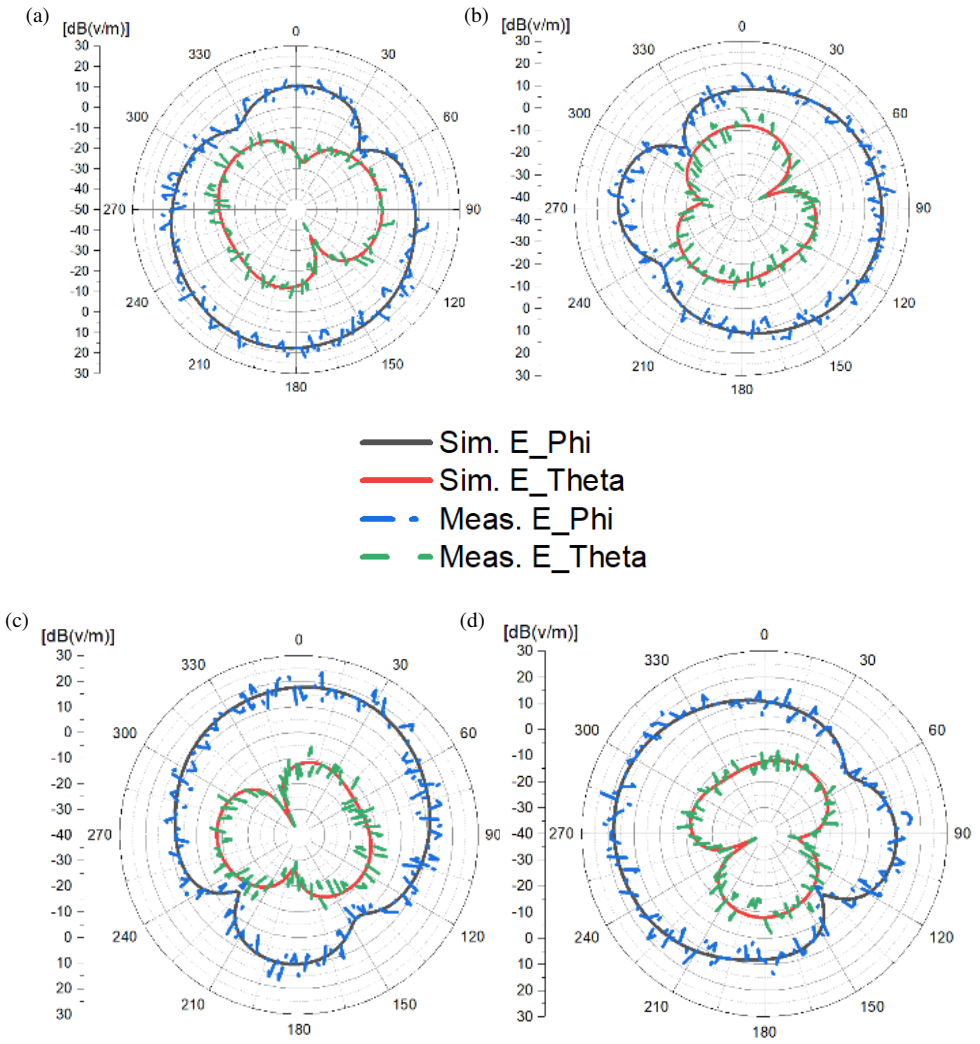

FIGURE 11. Patterns of electric radiation in two dimensions along the xy and yz-planes. (a) Ant-1; (b) Ant-2; (c) Ant-3; and (d) Ant-4.

subsequent equation can be solved to ascertain the guaranteed value of ECCs:

$$\mathrm{ECC}_{\mathrm{guaranteed}} = |\rho_{ij}|^2 \text{ guaranteed} \tag{8}$$

This approach for assessing the ECC between the two antennas is employed due to the designed MIMO system exhibiting efficiency exceeding 90% within their operational bands. The ECC values from the antennas have been calculated and are illustrated in Figure 9. According to the commonly acknowledged performance criterion (ECC < 0.5) for MIMO systems, radiators with ECC values below 0.02 in both operational bands are considered to comply [20].

The DG is another crucial parameter to consider when MIMO performance is evaluated. The DG metric measures the improvement in performance of the antenna array compared to a single element. The optimal dynamic range is 10 dB. Equation (9), as shown in Reference [20], calculates the DG to be 9.98 dB, as shown in Figure 9.

$$\mathrm{DG} = 10\sqrt{\left(1 - |0.99\rho_{ij}|^2\right)} \tag{9}$$

3.3. Performance of Radiation Patterns

The elements used in this paper mainly cover the top and bottom surfaces of the PCB with almost omnidirectional radiation patterns. The radiation patterns of four antennas (Ant. 1–Ant. 4) operating at 5, 5.25, 5.5, and 6 GHz are shown in Figure 10, which is a 3-dimensional accurate representation.

The radiation patterns of the C-shaped monopole antennas exhibit bidirectionality, generating electromagnetic waves in both forward and backward directions, resulting in a quasi-omnidirectional pattern. Directional antennas are preferred for communications that require a direct line of sight, while MIMO antennas are beneficial in circumstances with several paths and no direct line of sight. MIMO antenna design utilizes many signal routes to improve data throughput over numerous channels. As a result, the importance of antenna directivity for MIMO operations decreases.

Figure 11 depicts the two-dimensional electric radiation pattern of the antenna in the xy and yz-planes at a frequency of 5 GHz, explicitly showing the Co-Pol and X-Pol patterns. The radiation pattern was measured using a single port, while the

TABLE 1. Comparative analysis with previous studies.

Ref.	No. of antennas	PCB size (mm^2)	Frequency bands (GHz)	Isolation (dB)	Gain (dBi)	Efficiency (%)	ECC	Diodes per element	Switching Tech.
[21]	4	65×120	0.74–1.2, 1.1–2.42	> 12	-0.7–3.5	52–78	NM	2	PIN and Varactor
[22]	4	60×120	3.2–3.8	> 10	NM	NM	< 0.16	1	Varactor
[23]	4	60×120	1.3–2.6	> 12	-1.9–2.4	48–78	< 0.2	1	Varactor
[24]	4	50×50	4–4.35, 4.55–5.56	> 15	1.3–3.2, 3.5–4.4	45–68	< 0.07	1	Varactor
[25]	4	90×90	3–4.5, 4.4–6	> 15	3–4.4	50–70	< 0.15	1	PIN
[26]	4	70×70	2.5–5.2	> 20	1–1.7	60–91	< 0.3	1	PIN
[27]	4	38×50	3.2–3.4, 3.8–4.2, 5–6	> 15	3–3.4	NM	< 0.15	3	PIN
[28]	4	65×65	3.3–3.8, 4.4–5	> 15	2–4.5	60–92	< 0.13	4	PIN
[29]	4	68×68	2.4, 3.5, 5.5	> 18	1.4–5	80–83	< 0.18	8	PIN
Prop. work	4	40×40	4–5.18, 4.5–5.5, 5–6, 5.2–6.4, 5.45–6.65	> 18	3.8–4.3	94–97	< 0.02	1	Varactor

load on the other ports was kept at 50. A distance of one meter was kept between the suggested MIMO antennas and the transmitter antenna, causing signal strength changes depending on the antenna's movement in the xy- and yz-planes.

Compared to the E-theta cross-polarization components, the E-phi components, which align with the direction of the central lobe, are more intense. This characteristic enhances the planned MIMO system's practical effectiveness by improving pattern diversity and optimal polarization. The results from the simulations agree with those from the measurements.

The gain and total efficiency characteristics of a varactor diode in five distinct states are illustrated in Figure 12.

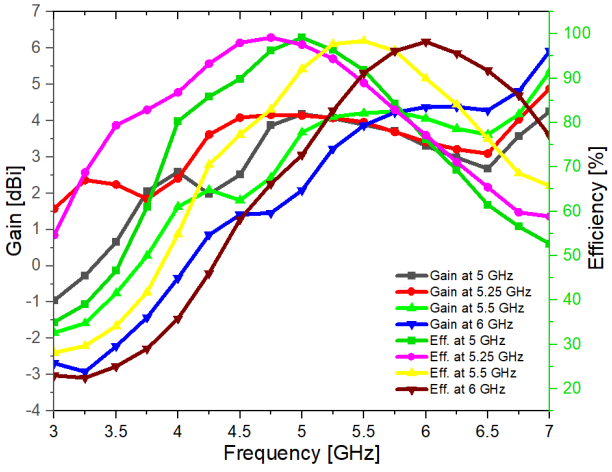

FIGURE 12. Total efficiency and realized gain for four frequencies.

These states have the following operating frequencies: 4.25–6.48 GHz, 5.18–5.18 GHz, 5.25–5.5 GHz, 5–6 GHz, and 5.45–6.65 GHz. The minimum gain and efficiency within these frequency ranges are determined to be 3.8 dBi and 94%, respectively. On the contrary, the maximal gain attains 4.3 dBi, accompanied by a peak overall efficiency of 97%. It is worth noting that as the frequency increases, the reconfigurable modified monopole C-shaped antenna demonstrates a significant enhancement in gain. Accounting for losses due to mismatching in impedance, conduction, and dielectric, the overall efficiency across the operating bands falls short of radiation efficiency by an approximate factor of 0.96.

4. COMPARISON WITH PREVIOUS REPORTED DESIGNS

The performance of the proposed antennas is evaluated by comparing them with previously reported designs. Table 1 thoroughly examines and presents several critical parameters, including the number of elements, ground clearance zone area, frequency bands, isolation of MIMO antennas, gain, ECC, and total efficiencies in multiple bands. It shows that the proposed sub-6 GHz/5G antennas have high-performance features, such as a small structure size ($40 \times 40\,mm^2$), a wide bandwidth, the ability to be used for future 5G MIMO applications, and a higher overall efficiency than other published works. Optimizing the parameters and ground plane structure was almost the same as $\lambda/2$, leading to a wide bandwidth that included five bands and a high efficiency of more than 94%.

The orthogonal antenna alignment allows for different radiation patterns, effectively isolating radiators by more than 18 dB without complicated decoupling parts and ensuring that the ECC is less than 0.02.

5. CONCLUSION

This paper introduces a four-port wide-band reconfigurable compact MIMO antenna system employing varactor diodes. The proposed antennas exhibit wide-band characteristics, offering frequency tuning across two bands: 4 to 5.18 GHz for lower biasing (0.5 V) and 5.45 to 6.65 GHz for higher biasing (10 V). By manipulating the varactor diode's biasing voltage, a continuous frequency sweep is achieved, facilitated by using a lumped capacitor to block alternate current coupling and direct current shorting.

The design comprises four orthogonal elements etched into the surface plane, incorporating rectangular-shaped DGS. Noteworthy attributes of this antenna design include its compact form factor ($40 \times 40\,\text{mm}^2$), planar geometry, low profile, cost-effectiveness, absence of radiation interference from biasing lines, and ease of manufacture.

Furthermore, the antenna demonstrates robust performance, with lower band isolation exceeding 18 dB and upper band isolation surpassing 20 dB. The antenna works well at changing frequencies over a wide range, staying stable, making enough radiation patterns, and getting good ECC values, as shown by both simulated and measured results. Consequently, the antenna holds promise for diverse applications, notably in software-defined and cognitive radios requiring frequency reconfigurability.

ACKNOWLEDGEMENT

The author appreciates Al-Iraqia University (https://aliraqia.edu.iq) for providing the research facilities to finish this work.

REFERENCES

[1] Singh, G., S. Kumar, B. K. Kanaujia, and V. K. Pandey, "Design and implementation of a compact tri-band four-port multiple-input-multiple-output antenna," *International Journal of RF and Microwave Computer-Aided Engineering*, Vol. 32, No. 8, e23218, 2022.

[2] Kareem, Q. H. and M. J. Farhan, "Miniaturized quad-port UWB-MIMO antenna with band-notched characteristics at 5 GHz," *Progress In Electromagnetics Research C*, Vol. 118, 263–275, 2022.

[3] Tütüncü, B. and M. Kösem, "Substrate analysis on the design of wide-band antenna for sub-6 GHz 5G communication," *Wireless Personal Communications*, Vol. 125, No. 2, 1523–1535, 2022.

[4] Hussain, R., A. Raza, M. U. Khan, A. Shammim, and M. S. Sharawi, "Miniaturized frequency reconfigurable pentagonal MIMO slot antenna for interweave CR applications," *International Journal of RF and Microwave Computer-Aided Engineering*, Vol. 29, No. 9, e21811, 2019.

[5] Majid, H. A., M. K. A. Rahim, M. R. Hamid, M. F. Ismail, and F. Malek, "Frequency reconfigurable wide to narrow band monopole with slotted ground plane antenna," *Journal of Electromagnetic Waves and Applications*, Vol. 26, No. 11-12, 1460–1469, 2012.

[6] Majid, H. A., M. K. A. Rahim, M. R. Hamid, and M. F. Ismail, "Frequency reconfigurable microstrip patch-slot antenna with directional radiation pattern," *Progress In Electromagnetics Research*, Vol. 144, 319–328, 2014.

[7] Alam, M. S. and A. M. Abbosh, "Wideband pattern-reconfigurable antenna using pair of radial radiators on truncated ground with switchable director and reflector," *IEEE Antennas and Wireless Propagation Letters*, Vol. 16, 24–28, 2017.

[8] Chattha, H. T., N. Aftab, M. Akram, N. Sheriff, Y. Huang, and Q. H. Abbasi, "Frequency reconfigurable patch antenna with bias tee for wireless LAN applications," *IET Microwaves, Antennas & Propagation*, Vol. 12, No. 14, 2248–2254, 2018.

[9] Li, K., Y.-M. Cai, Y. Yin, and W. Hu, "A wideband E-plane pattern reconfigurable antenna with enhanced gain," *International Journal of RF and Microwave Computer-Aided Engineering*, Vol. 29, No. 2, e21530, 2019.

[10] Khairnar, V. V., B. V. Kadam, C. K. Ramesha, and L. J. Gudino, "A reconfigurable parasitic antenna with continuous beam scanning capability in H-plane," *AEU — International Journal of Electronics and Communications*, Vol. 88, 78–86, 2018.

[11] Hossain, K., T. Sabapathy, M. Jusoh, P. J. Soh, R. B. Ahmad, M. I. Jais, M. N. Osman, M. N. M. Yasin, H. A. Rahim, N. Saluja, and Q. H. Abbasi, "A frequency-reconfigurable microstrip antenna with constant dipole-like radiation patterns using single bias, triple varactor tuning with reduced complexity," *Wireless Personal Communications*, Vol. 123, No. 2, 1003–1024, 2022.

[12] Rajagopalan, H., J. M. Kovitz, and Y. Rahmat-Samii, "MEMS reconfigurable optimized E-shaped patch antenna design for cognitive radio," *IEEE Transactions on Antennas and Propagation*, Vol. 62, No. 3, 1056–1064, 2014.

[13] Kovitz, J. M., H. Rajagopalan, and Y. Rahmat-Samii, "Design and implementation of broadband MEMS RHCP/LHCP reconfigurable arrays using rotated E-shaped patch elements," *IEEE Transactions on Antennas and Propagation*, Vol. 63, No. 6, 2497–2507, 2015.

[14] Lago, H., Z. Zakaria, M. F. Jamlos, and P. J. Soh, "A wideband reconfigurable folded planar dipole using MEMS and hybrid polymeric substrates," *AEU — International Journal of Electronics and Communications*, Vol. 99, 347–353, 2019.

[15] Abdulkawi, W. M., A.-F. A. Sheta, W. A. Malik, S. U. Rehman, and M. S. Alkanhal, "RF MEMS switches enabled H-shaped beam reconfigurable antenna," *Applied Computational Electromagnetics Society Journal*, Vol. 34, No. 9, 1312–1319, 2019.

[16] Xu, Z.-Q., Y.-T. Sun, Q.-Q. Zhou, Y.-L. Ban, Y.-X. Li, and S. S. Ang, "Reconfigurable MIMO antenna for integrated-metal-rimmed smartphone applications," *IEEE Access*, Vol. 5, 21 223–21 228, 2017.

[17] Lee, W.-W. and B. Jang, "A tunable MIMO antenna with dual-port structure for mobile phones," *IEEE Access*, Vol. 7, 34 113–34 120, 2019.

[18] Riaz, S., X. Zhao, and S. Geng, "A frequency reconfigurable MIMO antenna with agile feedline for cognitive radio applications," *International Journal of RF and Microwave Computer-Aided Engineering*, Vol. 30, No. 3, e22100, 2020.

[19] Pant, A., M. Singh, and M. S. Parihar, "A frequency reconfigurable/switchable MIMO antenna for LTE and early 5G applications," *AEU — International Journal of Electronics and Communications*, Vol. 131, 153638, 2021.

[20] Kareem, Q. H., R. A. Shihab, and H. H. Kareem, "Compact dual-polarized reconfigurable MIMO antenna based on a var-

actor diode for 5G mobile terminal applications," *Progress In Electromagnetics Research C*, Vol. 137, 185–198, 2023.

[21] Hussain, R. and M. S. Sharawi, "4-element planar MIMO reconfigurable antenna system for cognitive radio applications," in *2015 IEEE International Symposium on Antennas and Propagation & USNC/URSI National Radio Science Meeting*, 717–718, Vancouver, BC, Canada, 2015.

[22] Hussain, R. and M. S. Sharawi, "Reconfigurable pentagonal slot based 4-element MIMO antennas," in *2017 IEEE International Symposium on Antennas and Propagation & USNC/URSI National Radio Science Meeting*, 1151–1152, San Diego, CA, USA, 2017.

[23] Zhao, X. and S. Riaz, "A dual-band frequency reconfigurable MIMO patch-slot antenna based on reconfigurable microstrip feedline," *IEEE Access*, Vol. 6, 41 450–41 457, 2018.

[24] Kareem, Q. H., M. J. Farhan, and A. K. Jasim, "Design and analysis a frequency reconfigurable octagonal ring-shaped quad-port dual-band antenna based on a varactor diode," *Progress In Electromagnetics Research C*, Vol. 116, 235–248, 2021.

[25] Mathur, R. and S. Dwari, "Frequency and port reconfigurable MIMO antenna for UWB/5G/WLAN band IoT applications," *International Journal of RF and Microwave Computer-Aided Engineering*, Vol. 31, No. 7, e22692, 2021.

[26] Singh, G., S. Kumar, A. Abrol, B. K. Kanaujia, V. K. Pandey, M. Marey, and H. Mostafa, "Frequency reconfigurable quad-element MIMO antenna with improved isolation for 5G systems," *Electronics (Switzerland)*, Vol. 12, No. 4, 796, 2023.

[27] Abdullah, L. W., Q. H. Kareem, and A. H. Sallomi, "A quad-port multiple-input-multiple-output system for underlay or interweave cognitive radio," *Indonesian Journal of Electrical Engineering and Computer Science (IJEECS)*, Vol. 29, No. 3, 1480–1495, 2023.

[28] Thangarasu, D., S. K. Palaniswamy, and R. R. Thipparaju, "Quad port multipolarized reconfigurable MIMO antenna for sub 6 GHz applications," *International Journal of Antennas and Propagation*, Vol. 2023, No. 3, 1–17, 2023.

[29] Deepa, T. and T. R. Rao, "Quad element reconfigurable radiation pattern MIMO antenna for indoor wireless communication," *Progress In Electromagnetics Research Letters*, Vol. 112, 1–8, 2023.

[30] Balanis, C. A., *Antenna Theory: Analysis and Design*, 4th ed., John Wiley & Sons, Inc., 2016.

[31] Wang, Y., J. Li, and L.-X. Ran, "An equivalent circuit modeling method for ultra-wideband antennas," *Progress In Electromagnetics Research*, Vol. 82, 433–445, 2008.

[32] Paul, C. R., *Analysis of Multiconductor Transmission Lines*, 780, Wiley-IEEE Press, 2008.

[33] Kareem, Q. H. and M. J. Farhan, "Compact dual-polarized eight-element antenna with high isolation for 5G mobile terminal applications," *International Journal of Intelligent Engineering and Systems*, Vol. 14, No. 6, 187–197, 2021.